Cell Reports

Article

IP_3 Receptor-Dependent Cytoplasmic Ca^{2+} Signals Are Tightly Controlled by Cavβ3

Graphical Abstract

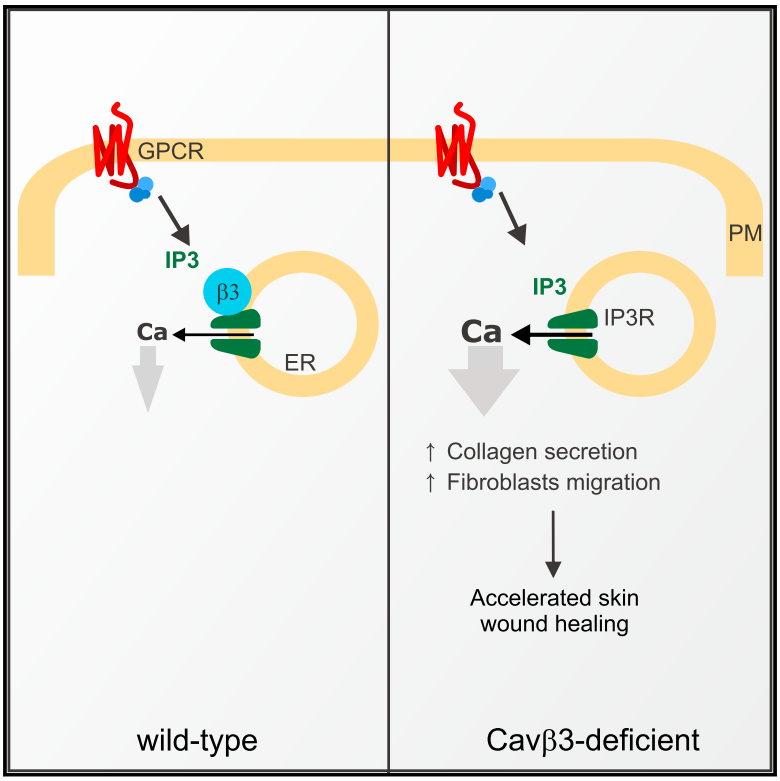

Highlights

- Cavβ3 protein binds to the IP_3 receptor and desensitizes cells to low IP3 levels
- Loss of the Cavβ3 protein leads to increased IP_3-dependent Ca^{2+} release
- Enhanced Ca^{2+} release translates into faster migration and more collagen secretion
- Mice lacking the *Cacnb3* gene show more efficient skin wound healing

Authors

Anouar Belkacemi, Xin Hui, Barbara Wardas, ..., Peter Lipp, Andreas Beck, Veit Flockerzi

Correspondence

veit.flockerzi@uks.eu

In Brief

Belkacemi et al. show that the calcium channel subunit Cavβ3 binds to the IP_3R and desensitizes cells to low IP_3 levels, influencing fibroblast migration and collagen secretion. Removal of the Cavβ3 protein in mice results in faster skin wound healing.

Belkacemi et al., 2018, Cell Reports *22*, 1339–1349
January 30, 2018
https://doi.org/10.1016/j.celrep.2018.01.010

CellPress

Cell Reports
Article

IP_3 Receptor-Dependent Cytoplasmic Ca^{2+} Signals Are Tightly Controlled by Cavβ3

Anouar Belkacemi,[1] Xin Hui,[2] Barbara Wardas,[1] Matthias W. Laschke,[3] Ulrich Wissenbach,[1] Michael D. Menger,[3] Peter Lipp,[2] Andreas Beck,[1] and Veit Flockerzi[1,4,*]
[1]Institut für Experimentelle und Klinische Pharmakologie und Toxikologie der Universität des Saarlandes, 66421 Homburg, Germany
[2]Institut für Molekulare Zellbiologie der Universität des Saarlandes, 66421 Homburg, Germany
[3]Institut für Klinisch-Experimentelle Chirurgie der Universität des Saarlandes, 66421 Homburg, Germany
[4]Lead Contact
*Correspondence: veit.flockerzi@uks.eu
https://doi.org/10.1016/j.celrep.2018.01.010

SUMMARY

Voltage-gated calcium channels (Cavs) are major Ca^{2+} entry pathways in excitable cells. Their β subunits facilitate membrane trafficking of the channel's ion-conducting α1 pore and modulate its gating properties. We report that one β subunit, β3, reduces Ca^{2+} release following stimulation of phospholipase C-coupled receptors and inositol 1,4,5-trisphosphate (IP_3) formation. This effect requires the SH3-HOOK domain of Cavβ3, includes physical β3/IP_3 receptor interaction, and prevails when agonist-induced IP_3 formation is bypassed by photolysis of caged IP_3. In agreement with β3 acting as a brake on Ca^{2+} release, fibroblast migration is enhanced *in vitro*, and *in vivo*, closure of skin wounds is accelerated in the absence of β3. To mediate specific physiological responses and to prevent Ca^{2+} toxicity, cytoplasmic Ca^{2+} signals must be tightly controlled. The described function of β3, unrelated to its function as a Cav subunit, adds to this tight control.

INTRODUCTION

Many physiological processes are regulated by changes of the cytoplasmic concentrations of calcium ions (Ca^{2+}), which are tightly regulated by Ca^{2+}-permeable ion channels, Ca^{2+} transporters, and pumps within the plasma membrane and the membranes of intracellular compartments. Major plasma membrane Ca^{2+} entry pathways include voltage-gated Ca^{2+} channels (Cavs) that comprise a pore-forming α1 subunit and the auxiliary subunits β, α2, δ, and, in skeletal muscle, γ (Catterall et al., 2005; Hofmann et al., 2014; Rima et al., 2016). These auxiliary subunits are essential in trafficking the pore-forming α1 to the plasma membrane (Dolphin, 2012), shaping current kinetics (He et al., 2007), permitting voltage-dependent channel activation (Kadurin et al., 2016), and controlling transsynaptic channel coupling (Fell et al., 2016).

The β subunits are cytosolic proteins encoded by four genes, *Cacnb1* to *Cacnb4*. They consist of a conserved core region flanked by non-conserved N and C termini (Buraei and Yang, 2013). Differential splicing of the primary transcripts gives rise to a variety of N termini for each of the four genes. Their core regions encode a Src homology (SH) 3 and a guanylate kinase (GK) domain linked by a HOOK domain. The GK domain contains the α1-binding pocket, which binds with high affinity a conserved sequence located in the cytoplasmic loop of the pore-forming α1 subunits of the high-Cavs (Chen et al., 2004; Opatowsky et al., 2004; Van Petegem et al., 2004). In the absence of Cavα1 proteins, most β subunits reside in the cytoplasm; only the palmitoylated β2-N3 (Qin et al., 1998) and the β2-N5 (Kim et al., 2015; Miranda-Laferte et al., 2014) are tethered to the plasma membrane.

Bound or unbound to the ion-conducting Cavα1, the β subunits can interact with additional proteins (Buraei and Yang, 2010; Rima et al., 2016). Following skeletal muscle excitation, Cav1.1 and the Cav1.1-bound β1a interact with a cytosolic domain of the ryanodine receptor type 1 (RyR1) (Cheng et al., 2005; Flucher et al., 2005; Rebbeck et al., 2015; Szpyt et al., 2012) and thereby trigger Ca^{2+} release from the sarcoplasmic reticulum. This conformational coupling is the underlying mechanism for excitation-contraction coupling in skeletal muscle. In the brain β proteins interact with monomeric GTP-binding proteins Rad, Rem, Rem2, and Gem/Kir (Béguin et al., 2001, 2007; Fan et al., 2012; Yang and Colecraft, 2013) and a β-anchoring and β-regulatory protein (BARP) (Béguin et al., 2014). The distinct β4 splice variants modulate channel function and accumulate in the nucleus, where they recruit transcription factors and regulate gene expression (Etemad et al., 2014; Hibino et al., 2003; Tadmouri et al., 2012).

The β3 subunit is preferentially associated with L-type (Cav1.2α1) and N-type Ca^{2+} channels (Cav2.2α1) (Müller et al., 2010; Murakami et al., 2002; Namkung et al., 1998) in the brain (Ludwig et al., 1997), smooth muscle (Held et al., 2007), and endocrine cells (Berggren et al., 2004; Freise et al., 1999). Additional β3 functions not related to Cavs include blunting of N-methyl-D-aspartate receptor (NMDAR)-2B-induced activities in the hippocampus (Jeon et al., 2008) and an abridged Ca^{2+} mobilization from intracellular stores and lower frequencies of glucose-induced intracellular Ca^{2+} oscillations in pancreatic β cells (Berggren et al., 2004).

In this study we investigated the roles of β3 in Ca^{2+} release from intracellular stores and identified primary fibroblasts as an appropriate cellular system. The *Cacnb3* gene is expressed in these cells, whereas depolarization-induced Ca^{2+} influx is

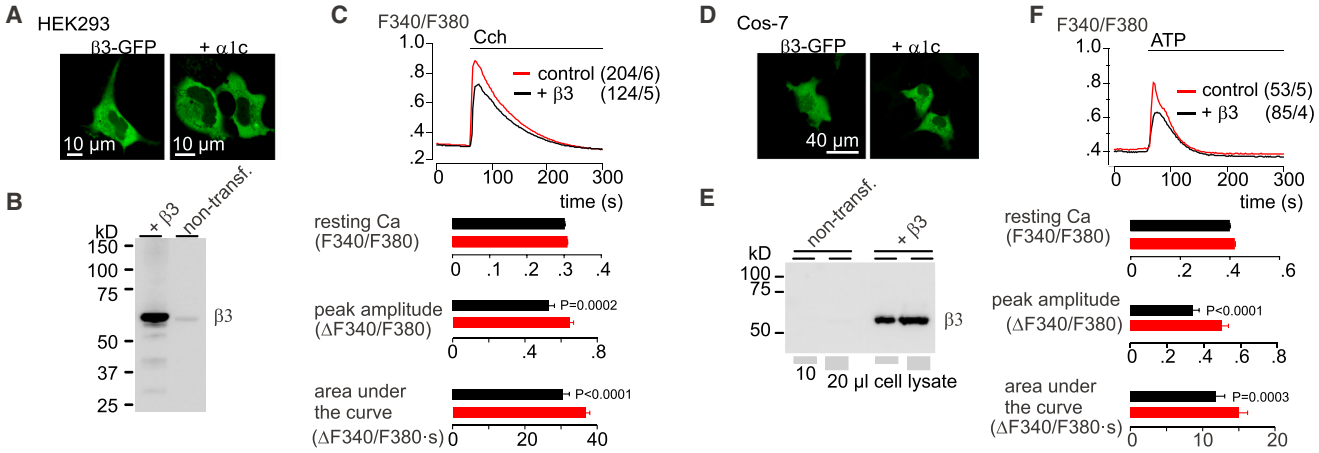

Figure 1. Decreased Agonist-Induced Calcium Release in β3 cDNA-Expressing Cells

(A and D) Confocal images of HEK (A) and Cos-7 (D) cells expressing the GFP-tagged Cavβ3 cDNA in the absence (left) and presence (right) of the α1c (Cav1.2) cDNA.

(B and E) Western blot of protein lysates from HEK (B) and Cos-7 (E) cells, non-transfected or transfected with Cavβ3 cDNA (+β3).

(C and F) Fura-2 ratio (F340/F380) over time before and after addition of carbachol (Cch) in HEK cells (C) or ATP in Cos-7 cells (F) in the absence of extracellular Ca^{2+}. Control (red), cells transfected with the GFP cDNA only; +β3 (black), cells transfected with Cavβ3-IRES-GFP cDNA; (number of cells/independent experiments). Resting Ca^{2+} in the cytoplasm, peak amplitude, and area under the curve are presented below the traces as means ± SEM; p values were calculated using a Mann-Whitney test or unpaired two-tailed Student's t test.

See also Figures S1 and S2.

hardly detectable, allowing the evaluation of β3 functions unrelated to voltage-gated Ca^{2+} currents. We show that in response to physiological agonists or upon photolysis of caged inositol 1,4,5-trisphosphate (IP_3), Ca^{2+} release from intracellular stores is increased in fibroblasts from β3 knockout (KO) mice and in Cos-7 cells, which do not express endogenous β3 compared with controls, wild-type fibroblasts, and Cos-7 cells transfected with β3 cDNA. The amount of the IP_3 receptor (IP_3R) protein does not depend on the presence of β3, but both proteins, IP_3R and β3, are co-immunoprecipitated. Both the endogenous and recombinant β3 protein efficiently reduce the IP_3R's binding of IP_3. As a result, cells are less sensitive to low IP_3 concentrations followed by changes in fibroblast migration *in vitro*, in collagen secretion, and in skin wound healing *in vivo*. In summary, our results indicate that β3, unrelated to its role as a Ca^{2+} channel subunit, specifically modulates the cell's IP_3 sensitivity and thereby efficiently tunes agonist-induced cytoplasmic Ca^{2+} signals and cellular functions.

RESULTS

Cavβ3 Protein Interferes with Agonist-Induced Ca^{2+} Release

As described (Béguin et al., 2014; Suh et al., 2012), the wild-type β3 subunit is distributed throughout the cytoplasm, in both the absence and presence of a Cavα1 (Figures 1A, 1D, S1A, and S1B). In HEK293 (HEK) and Cos-7 cells transfected with the Cavβ3 cDNA, the β3 protein corresponds to ~55 kDa (Figures 1B and 1E). A protein of similar size, apparently endogenous β3, is detectable as a faint band in non-transfected HEK but not in non-transfected Cos-7 cells by the anti-β3 antibody (Figures 1B and 1E). In the presence of carbachol (Cch) or ATP, muscarinic receptors and P2Y receptors are stimulated in HEK and in Cos-7 cells, respectively, leading to PLC activation and cleavage of phosphatidyl inositol 4,5-bisphosphate (PIP_2) into IP_3 and diacylglycerol. IP_3 is bound by the IP_3R, Ca^{2+} is released from intracellular stores, mainly the endoplasmic reticulum (ER), and the cytoplasmic [Ca^{2+}] increases. This increase is monitored by Fura-2 and characterized as peak amplitude and area under the trace (Figures 1C and 1F) in non-transfected HEK and Cos-7 cells (red trace) and in cells transfected with the β3 cDNA (black trace). Expression of β3 cDNA significantly reduces the increase of cytoplasmic [Ca^{2+}].

Primary fibroblasts isolated from embryonic mice do express the *Cacnb3* gene; the β3 protein is present (Figure 2A). It is absent in fibroblasts isolated from *Cacnb3*-deficient (β3 KO) mice (Figure 2A). Depolarization of Fura-2-loaded fibroblasts by high potassium (74 mM) in the presence of extracellular Ca^{2+} did not reveal any significant increase of cytoplasmic [Ca^{2+}], in neither wild-type nor β3 KO cells (Figure 2B), indicating the absence of depolarization-induced Ca^{2+} influx through Cavs. In contrast, application of high potassium on HEK cells co-expressing the cDNA of Cav1.2 (α1c) and β3 or on acutely isolated mouse cardiomyocytes (Figures S1C and S1D) induced immediate Ca^{2+} increase, which was reduced by the Ca^{2+} channel blocker nimodipine. Whole-cell recordings from wild-type and β3 KO fibroblasts revealed minuscule voltage-gated currents (Figure S1E; current density, I_{Ca10mV}, −2.25 ± 0.44 pA/pF; n = 10) with no significant difference between wild-type and β3 KO cells (Figures S1E and S1F). Bradykinin (BK) and lysophosphatidic acid (LPA) stimulate BK and LPA receptors in fibroblasts (Vogt

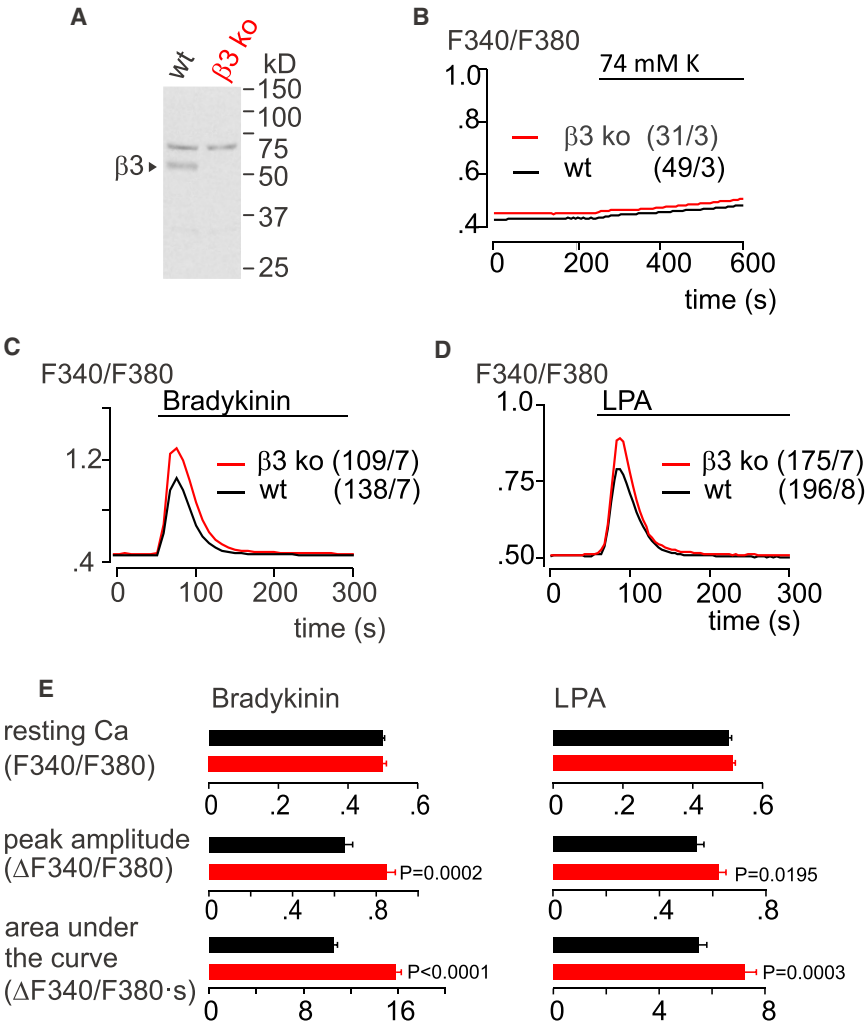

Figure 2. Increased Agonist-Induced Calcium Release in Cavβ3 KO Mouse Fibroblasts

(A) Western blot of protein lysates from primary fibroblasts isolated from wild-type (WT) and β3 KO mice.

(B) No increase in cytoplasmic [Ca^{2+}] detectable in WT and β3 KO cells upon potassium-induced depolarization in the presence of extracellular Ca^{2+} (2 mM).

(C and D) Fura-2 (F340/F380) ratiometric traces in the absence of extracellular Ca^{2+} before and after addition of bradykinin (10 μM; C) or LPA (20 μM; D) in wild-type (black) and β3 KO (red) fibroblasts (number of cells/ number of experiments).

(E) Summary of resting Ca^{2+} in the cytoplasm, peak amplitude, and the area under the curve from experiments shown in (C) and (D). Data are presented as mean ± SEM; p values were calculated using a Mann-Whitney test.

See also Figures S1 and S2.

et al., 2003), followed by IP_3-dependent Ca^{2+} release. Resting cytoplasmic [Ca^{2+}] prior to agonist application was not significantly different in wild-type and β3 KO fibroblasts, but the agonist-induced Ca^{2+} increase was significantly higher in β3 KO fibroblasts compared with control wild-type cells (Figures 2C–2E). This Ca^{2+} release in fibroblasts and in Cos-7 cells was absent in the presence of the phospholipase C inhibitor U73122 (Figures S2A and S2B). The elevation of cytoplasmic [Ca^{2+}] following Ca^{2+} store depletion in the presence of thapsigargin was not different in fibroblasts from either genotype (Figure S2C), indicating that the Ca^{2+} content of intracellular stores was not compromised in the absence of β3.

The agonist-induced Ca^{2+} release upon receptor stimulation is larger in β3 KO compared with wild-type fibroblasts, and store-operated Ca^{2+} entry (Putney and Bird, 1993) might be different in these cells. The stores were first depleted in the presence of the agonist LPA but in the absence of extracellular Ca^{2+}, as in Figure 2D (Figure S2D). After return of cytoplasmic [Ca^{2+}] to baseline, extracellular Ca^{2+} was added, leading to Ca^{2+} entry through plasma membrane channels. This store-operated Ca^{2+} entry was not different in wild-type and β3 KO fibroblasts (Figure S2D) as were the inward currents, which developed after store depletion by IP_3 in the patch pipette (Figures S2E and S2F). These experiments demonstrate that β3 interferes with agonist-evoked Ca^{2+} release from the ER without affecting basal cytoplasmic [Ca^{2+}], Ca^{2+} content of the intracellular stores, or Ca^{2+} entry following Ca^{2+} store depletion.

Loss of Cavβ3 Sensitizes Cells to Low IP_3 Levels

To differentiate between the hypotheses that Cavβ3 interferes with the signal transduction pathway stimulated by the receptor or directly modulates IP_3R function, cells were loaded with membrane-permeable caged IP_3 and the fluorescent Ca^{2+} indicator Fluo-4. Care was taken to ensure equal loading by plating cells of different genotypes on the same coverslip (Figures 3 and S3). IP_3 was released by photolysis and subsequently activated the IP_3Rs, resulting in an increase of cytoplasmic [Ca^{2+}], which was monitored by Fluo-4. As shown in Figure 3A, UV light flashes of increasing energy enhanced Fluo-4 fluorescence in wild-type fibroblasts (black traces) and β3 KO fibroblasts (red traces). The Ca^{2+}-induced fluorescence was plotted versus the amount of flash energy as a measure for the amount of released IP_3 (Figure 3A). Also under this condition, the wild-type fibroblasts were less sensitive to IP_3 than β3 KO fibroblasts.

Cos-7 cells, which lack endogenous β3 (Figure 1E), were loaded with Fluo-4 and caged IP_3 and subsequently exposed to UV light flashes (Figure S3, bottom). As shown in Figure 3B, non-transfected Cos-7 cells (control) are more sensitive to IP_3 than the transfected cells (+β3) and thereby behave like the β3 KO fibroblasts (Figure 3A).

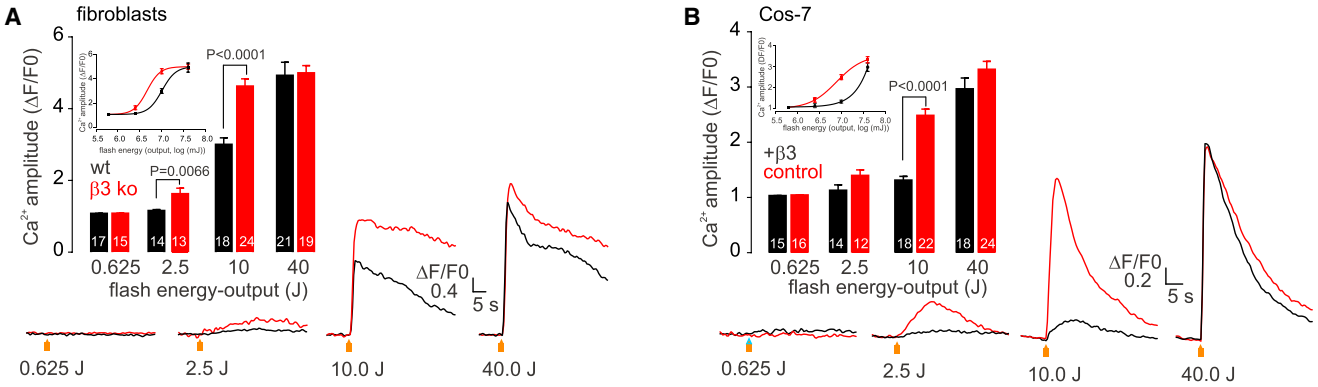

Figure 3. Cavβ3 Desensitizes Cells to Low Concentrations of IP_3

(A and B) Fibroblasts isolated from wild-type (WT; black) and β3 KO (red) mice (A) and Cos-7 cells (B), non-transfected (control; red) and transfected with β3 cDNA (+β3; black); cDNAs were loaded with caged IP_3 and Fluo-4/AM. IP_3 was released by UV flash photolysis at the indicated energies, and the cytoplasmic [Ca^{2+}] was monitored by Fluo-4 fluorescence. Bar graph showing Ca^{2+} amplitude ($\Delta F/F_0$) at the indicated energies (inset, Ca^{2+} amplitude-energy-dose-response curves). Data are presented as mean ± SEM, and the numbers of measured cells are indicated in the bars. Both genotypes (in one dish) at a given UV light flash energy were compared; the p values were calculated using unpaired two-tailed Student's t test.
See also Figures S3 and S5.

Interaction of Cavβ3 with the IP_3R

Mouse fibroblasts predominantly express the type 3 IP_3R gene (Figure S4A), and the IP_3R protein levels are not different in wild-type and β3 KO cells (Figure 4A). To verify a physical interaction of β3 and the IP_3R, both proteins were effectively co-immunoprecipitated by using the antibodies for β3 and the type 3 IP_3R (Figure 4B), the type1 and type 2 IP_3Rs (Figures S4B and S4C). To identify the β3 domain (Figure 4C) required for IP_3R binding, the deletion mutants β3-HOOK-$SH3_{\beta5}$-GK (β3ΔSH3) and β3-$SH3_{\beta1-\beta4}$-HOOK-$SH3_{\beta5}$ (β3ΔGK) were co-expressed with the type 3 IP_3R. As shown in Figures 4D and 4E, the β3ΔGK was still co-immunoprecipitated with the IP_3R and vice versa, but the β3ΔSH3 was not. To evaluate whether the effect of the full-length β3 protein on IP_3-induced Ca^{2+} release was maintained by β3 lacking the SH3 domain, the β3ΔSH3 were expressed in Cos-7 cells, and the presence of protein was controlled by western blot (Figure 4F). As shown in Figures 4G and 4H, the ATP-induced elevation of cytoplasmic [Ca^{2+}] was not different in β3ΔSH3 cDNA-expressing Cos-7 cells and in control cells, indicating that the SH3 domain is required for the decrease of agonist-induced Ca^{2+} release that had been observed with the full-length β3 protein.

All β subunits constitute a similar domain structure, and to evaluate whether the observed effect on IP_3-induced Ca^{2+} release is a specific property of β3, Cos-7 cells were transfected with two splice variants of β2, β2-N3, or β2-N4. No endogenous β2 protein was detectable in Cos-7 cells by an anti-β2 antibody (Link et al., 2009). The amino acid sequences of both proteins differ in their N terminus (Figure S5A), which determines that β2-N3 is associated with the plasma membrane (Figure S5B) by palmitoylation, whereas β2-N4, like β3, is distributed throughout the cell (Figure S5D). After loading cells with caged IP_3 and Fluo-4 and photolysis, as in Figures 3B and S3 (bottom), there were no significant differences in the IP_3 responses of non-transfected and β2-transfected Cos-7 cells (Figures S5C and S5E), indicating a β3-specific effect.

Cavβ3 Reduces IP_3 Binding by the IP_3R

The previous data show that β3 modulates IP_3-induced Ca^{2+} release and that β3 and IP_3R proteins do physically interact. Cerebellum microsomes, a rich source of IP_3Rs, were prepared from wild-type and β3 KO mice (Figure 5A) to study [^{3}H]IP_3 binding to the IP_3R. The equilibrium dissociation constants (K_d) of specific IP_3 binding by the IP_3R were significantly reduced in β3 KO microsomes (β3 KO, 9.78 ± 0.53 nM, n = 3; wild-type, 27.51 ± 5.40 nM, n = 3; p = 0.03) with no significant difference of the density of binding sites (β3 KO, Bmax 1.49 ± 0.15 pmol/mg, n = 3; wild-type, 2.26 ± 0.37 pmol/mg, n = 3; p = 0.12) (Figures 5B–5D). Next, binding of IP_3 to the IP_3R in mouse cerebellum microsomes (isolated from β3 KO mice) was measured either in the absence or presence of recombinant β3 protein. The amount of β3 protein per single fibroblast was estimated to be in the 10–100 nM range (Figures S4D and S4E). The β3 protein (Figure 5E, right) at 0.1 and 0.3 μM but not GST (at 1 μM; Figure 5E, left) reduced specific IP_3 binding compared with control (Figure 5F). Taken together, these results show that endogenously present as well as added recombinant β3 protein reduces the affinity of the IP_3R for IP_3. IP_3 binds to the IP_3-binding domain (IP_3BD) (Fan et al., 2015; Hamada et al., 2017), which covers most of the N-terminal 604 amino acid residues of the IP_3R type 3 (Figure 5G). Both β3 and IP_3BD cDNAs were co-expressed in Cos-7 cells, and immunoprecipitation was performed with anti-β3 and anti-IP_3BD. Both antibodies retained their target and the respective associated protein IP_3BD and β3 (Figure 5H). To monitor IP_3 binding by the IP_3BD in the presence of β3 but in the absence of any other proteins, both proteins were generated in *E. coli* (Figures 5E and 5I). Recombinant IP_3BD specifically binds IP_3 in a concentration-dependent manner, and binding was reduced in the presence of 0.2 μM β3 (Figure 5J). Specific

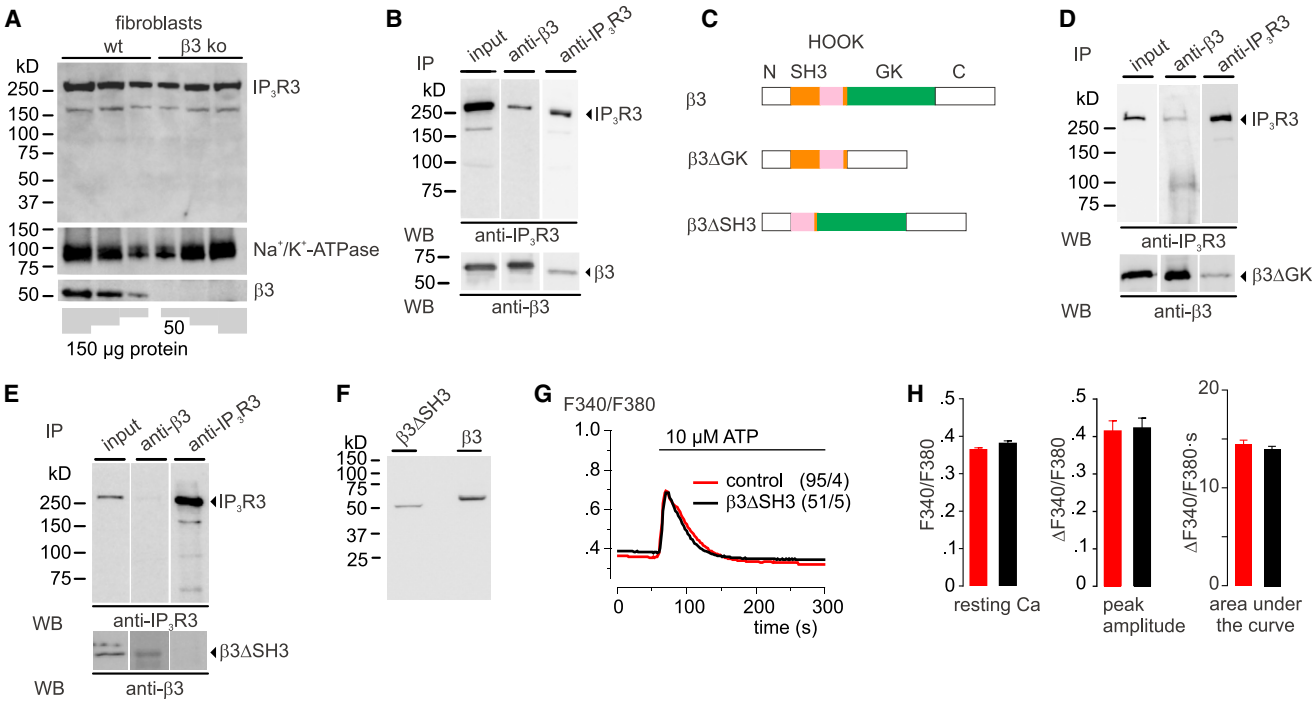

Figure 4. Cavβ3 Interacts with the IP_3R

(A) Western blots with increasing amount of protein from wild-type and β3 KO fibroblasts were probed subsequently with antibodies for IP_3R3, Na^+/K^+-ATPase, and β3.

(B) Co-immunoprecipitation of β3 and the IP_3R3. Lane 1, input (cell lysate); immunoprecipitation with the antibody for β3 (lane 2) and IP_3R3 (lane 3). Western blots with antibody for IP_3R3 (top) and β3 (bottom).

(C) Domain structure of β3, β3ΔGK (β3-$SH3_{[\beta1-\beta4]}$-HOOK-$SH3_{[\beta5]}$) and β3ΔSH3 (β3-HOOK-$SH3_{[\beta5]}$-GK).

(D and E) Western blots after co-immunoprecipitation of IP_3R3 and β3ΔGK (D) or β3ΔSH3 (E) using the antibodies as indicated.

(F) Western blot confirming expression of the β3ΔSH3 cDNA in Cos-7 cells.

(G) Fura-2 ratio (F340/F380) over time before and after stimulation with ATP (10 μM) in the absence of extracellular Ca^{2+} in Cos-7 cells expressing the β3ΔSH3-IRES-GFP cDNA (β3ΔSH3; black) and control cells expressing the GFP cDNA (red).

(H) Resting cytoplasmic Ca^{2+}, peak amplitudes, and area under the curve are shown as mean ± SEM; statistical significance was assessed using unpaired two-tailed Student's t test for resting cytoplasmic Ca^{2+} and peak amplitude and Mann-Whitney test for area under the curve.

See also Figure S4.

[^{3}H]IP_3 binding by the IP_3BD protein was reduced in the presence of β3-GST at increasing concentrations but not in the presence of GST alone, whereas recombinant β3-GST or GST did not bind IP_3 by themselves (Figure 5K).

Cavβ3 Function in Fibroblast Migration and Wound Healing

To shed light on the physiological role of β3 as a "brake" on IP_3-induced Ca^{2+} release in fibroblasts, which have the ability to migrate (Sixt, 2012), scratch assays were performed. The β3 KO fibroblasts showed significantly enhanced motility compared with wild-type cells (Figure 6A). This increased migration was retained when reducing the concentration of fetal calf serum from 10% (Figure 6B) to 1% (Figure 6C) and was not related to changes in proliferation or viability (Figures S6A and S6B), which were not significantly different for fibroblasts of both genotypes. Activation of focal adhesion kinase (FAK) and of myosin light chain (MLC) is associated with active movement of cells (Totsukawa et al., 2004; Zhao et al., 2016). The amounts of phosphorylated FAK and MLC were significantly increased in the β3 KO fibroblasts (Figures 6D and 6E), whereas staining of migrating fibroblasts for myosin IIa and for actin filaments and the amount of myosin IIa and the G-actin/F-actin ratio were not different (Figures S6C–S6F).

Fibroblasts play a crucial role in the final steps of wound repair and tissue remodeling (Gurtner et al., 2008). The β3 KO fibroblasts showed faster migration *in vitro* (Figures 6A–6C) and secreted more collagen compared with wild-type control cells (Figure 6F). Cavβ3 protein is also present in primary skin fibroblasts from wild-type mice (Figure 6G). Therefore we applied a defined circular wound of 2 mm diameter by removing the complete skin with epidermis and dermis on the shaved back of wild-type and β3 KO mice. For intravital microscopy, the dorsal skinfold chamber preparation was used, and the wound area in the skinfold chamber was photographed directly after wounding (day 0) and 3, 6, 10, and 14 days post-wounding (Figure 6H). Thereafter, the sizes of the wound areas were determined by digital images, and size on a given day was expressed as a percentage of the initial wound area. The process of wound closure continued for 14 days in both genotypes, but wound closure

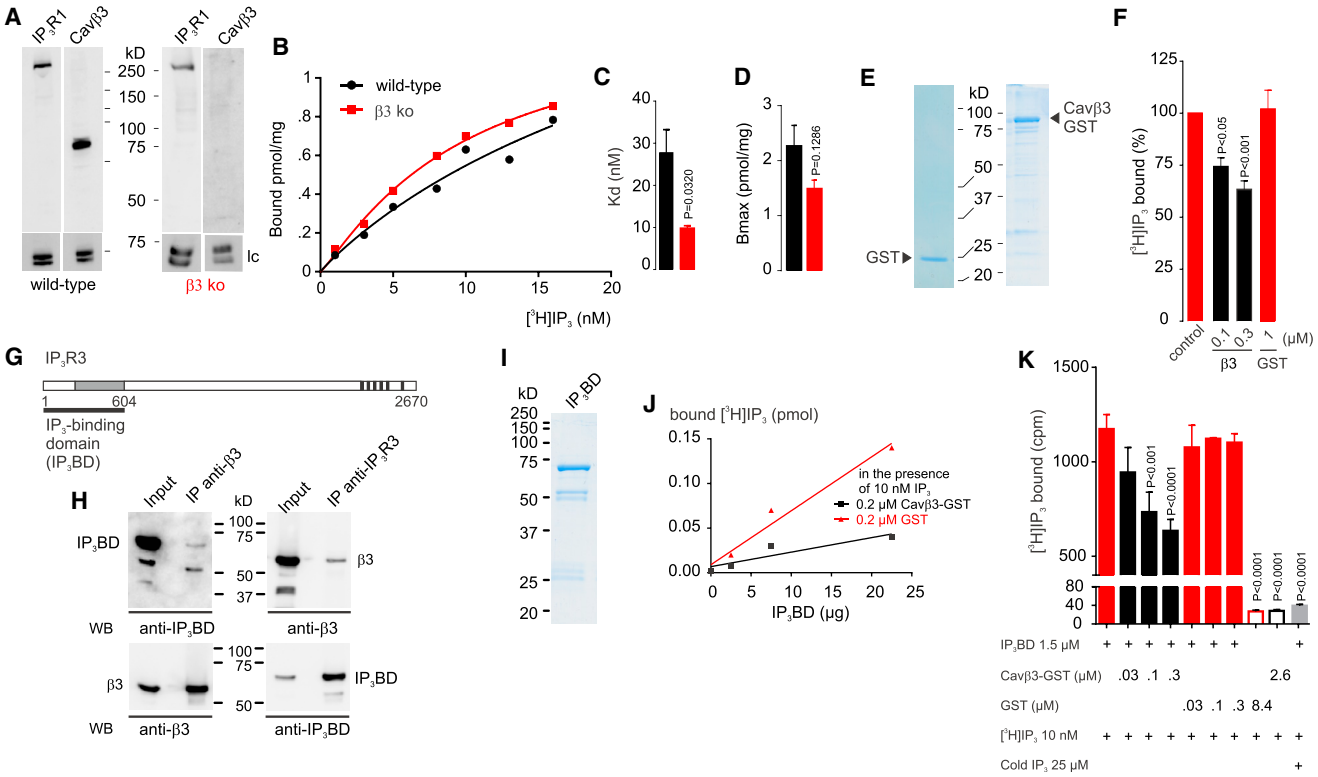

Figure 5. The β3 Protein Reduces IP_3 Binding to the IP_3R

(A) Western blot of microsomal proteins from wild-type (left) and β3 KO (right) mouse cerebellum using anti-β3, anti-IP_3R1, and anti-β2 (lc, loading control) antibodies.

(B–D) Equilibrium saturation binding of [^{3}H]IP_3 in the absence and presence of 25 μM unlabeled IP_3 by cerebellum microsomes prepared from wild-type (black) and β3 KO (red) mice. (B) A representative experiment out of three is shown with K_d (C) and Bmax (D) values as indicated. Data are shown as mean ± SEM, and p values were calculated using unpaired two-tailed Student's t test.

(E and F) Coomassie-stained recombinant GST and β3-GST (E) and [^{3}H]IP_3 (10 nM) (F) binding in the absence and presence of 25 μM IP_3 (non-specific binding was <40 cpm) by β3 KO cerebellum microsomes in the absence (control; 100% amounts to 0.66 ± 0.04 pmol/mg protein) and presence of recombinant β3-GST or GST as indicated. Data are shown as means ± SEM; n = 2 independent experiments in triplicate. p values were calculated using one-way ANOVA and Bonferroni's multiple comparisons test.

(G) Domain structure of IP_3R indicating the suppressor domain followed by the IP_3-binding domain (amino acids 1–604); six transmembrane domains are indicated in black.

(H) Co-immunoprecipitation of β3 and IP_3RBD (both cDNAs were co-expressed in Cos-7 cells) using anti-Cavβ3 and anti-IP_3R3 antibodies for immunoprecipitation and western blot as indicated.

(I) Coomassie-stained recombinant IP_3BD.

(J and K) Specific binding of [^{3}H]IP_3 (10 nM) (J) by recombinant IP_3BD (2.50, 7.50, and 22.50 μg) in the presence of 200 nM GST protein or 200 nM GST-β3 protein. (K) Specific [^{3}H]IP_3 binding to recombinant IP_3RBD (1.50 μM) in the absence (1,173.88 ± 76.48 cpm) or presence of GST and GST-β3 at increasing concentrations. Non-specific binding in the presence of 25 μM IP_3 (39.40 ± 2.76 cpm) and binding to GST-β3 or GST as indicated. Data are shown as means ± SEM; p values were calculated using one-way ANOVA and Bonferroni's multiple comparisons test.

See also Figure S4.

was significantly accelerated in β3 KO mice compared with wild-type controls (Figures 6H and 6I).

DISCUSSION

The release of Ca^{2+} from intracellular stores is crucial for elevating cytoplasmic [Ca^{2+}] and for shaping the spatiotemporal profile of cellular Ca^{2+} signals required to induce specific physiological responses. Our results that the Cavβ3 subunit tunes agonist-induced Ca^{2+} release offers further insights into the regulation of cellular Ca^{2+} signaling. In three distinct cell types, HEK and Cos-7 cells and fibroblasts isolated from mice (Figures 1 and 2), this effect of β3 was unrelated to its role as a Cav subunit. It prevailed when receptor stimulation by an agonist was bypassed by loading cells with caged IP_3 and releasing IP_3 through graded photolysis (Figure 3). Because the β3 subunit and the IP_3R were co-immunoprecipitated (Figure 4) and β3 efficiently reduced binding of IP_3 by the IP_3R (Figure 5) without binding IP_3 by itself, cells are less sensitive to IP_3 in the presence of β3. This role appears not to require presence and activity of Cavs, which underlie miniscule Ca^{2+} currents in primary fibroblasts (Figure S1) and which are not affected in the absence of β3. Fibroblasts are migrating cells and in agreement with β3 acting as a brake on Ca^{2+} release, migration in wild-type

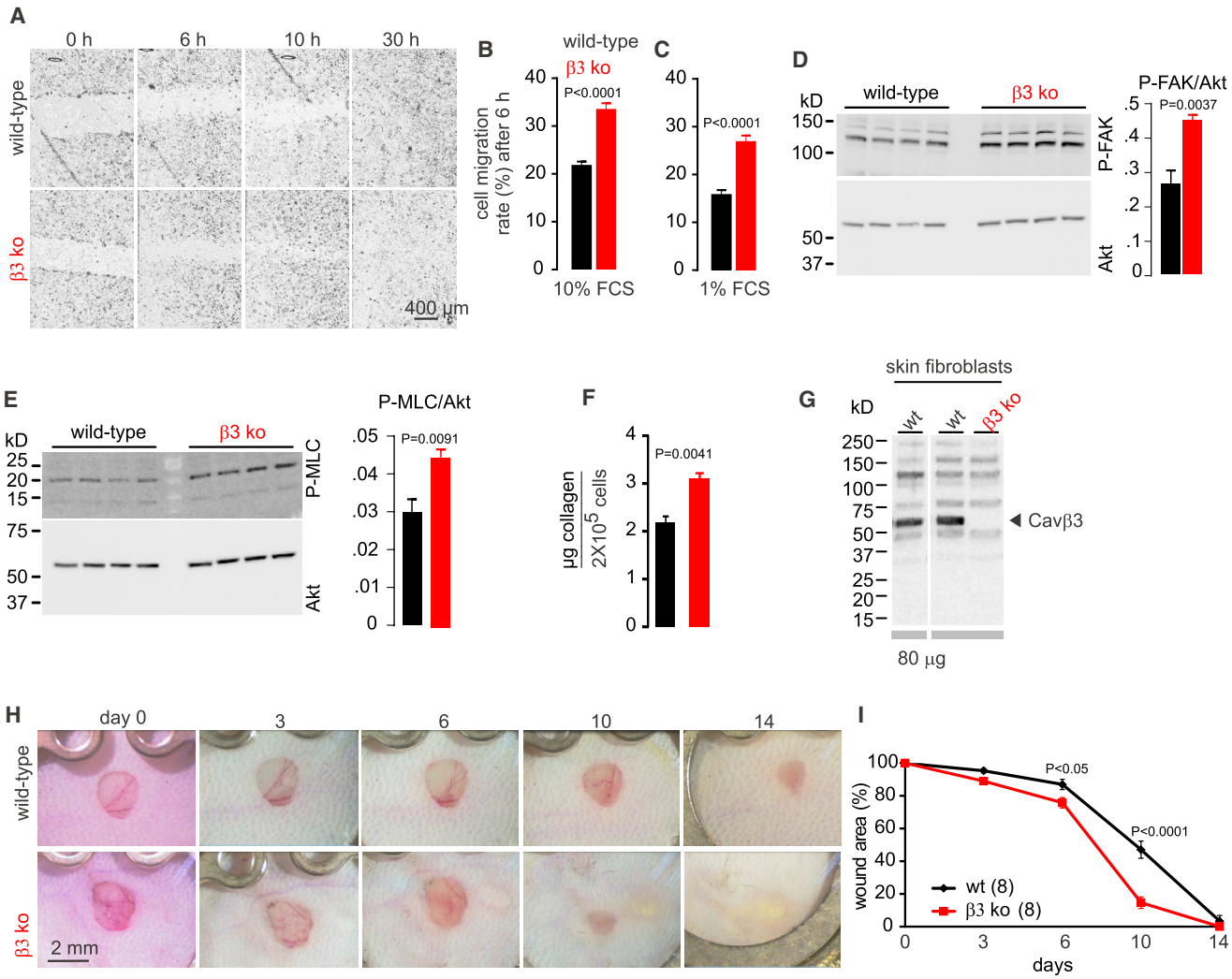

Figure 6. *In Vitro* Fibroblast Migration and *In Vivo* Wound Healing

(A) Representative images of migration from wild-type and β3 KO fibroblasts.

(B and C) Summary of cell migration rate calculated relative to the initial scratch area after 6 hr showing increased migration of β3 KO fibroblasts (red) compared with wild-type fibroblasts (black) in the presence of 10% fetal calf serum (FCS) (B) or 1% FCS (C). Data are shown as mean ± SEM, with the experiment performed three times with three independent cell preparations (32–40 images from three independent experiments; p values were calculated using unpaired two-tailed Student's t test).

(D and E) Western blot of wild-type and β3 KO primary fibroblasts using anti-P-FAK (Sr732) (D), P-MLC (E), and anti-Akt antibody as a loading control. Bar graphs show the densitometric quantification of the intensity of the corresponding immunostain as mean ± SEM; p values were calculated using unpaired two-tailed Student's t test.

(F) Collagen secretion from wild-type (black) and β3 KO fibroblasts (red) expressed as the mean ± SEM (n = 3 independent experiments; p values were calculated using unpaired two-tailed Student's t test).

(G) Western blot of wild-type and β3 KO primary skin fibroblasts lysates (80 μg per lane) using anti-β3 antisera.

(H) Images obtained from the skinfold chamber directly after wounding (day 0) and on days 3, 6, 10, and 14 post-wounding. The continuous process of wound closure, with complete epithelialization, is shown over 14 days in both genotypes.

(I) At the time points indicated, the wound area was determined and plotted as a percentage of the wound area on day 0 (immediately after wounding). Data are shown as mean ± SEM (n = 8 mice; p values were calculated using two-way ANOVA and Bonferroni's multiple comparisons test). Wound closure is significantly accelerated in β3 KO mice.

See also Figure S6.

fibroblasts was reduced *in vitro*, whereas *in vivo*, closure of a skin wound was accelerated in the absence of β3 (Figure 6).

The β3 subunit shares the common SH3-HOOK-GK core structure with other β subunits (Chen et al., 2004; Opatowsky et al., 2004; Van Petegem et al., 2004) but neither β2-N3 nor β2-N4 (also dubbed β2a and β2b) can replace β3 as a modulator of the IP_3R (Figure S5). Compared with the β3 amino acid sequence the β2 proteins differ substantially in their N and

C termini and within their HOOK domain, which covers 98 amino acid residues. It comprises stretches of serine, acidic, and basic residues required for β2 to associate with phospholipids, including PIP2 (Park et al., 2017), and which are absent or poorly conserved in the 49 amino acid HOOK domain of β3.

Canonical SH3 domains comprise five sequential β strands and mediate specific protein-protein interactions by binding to PxxP-containing motifs that are present but not conserved in the amino acid sequences of the murine IP_3Rs type 3 (one PxxP motif), type 2 (one), and type 1 (nine). In the Cavβ subunits, the four initial β strands of the SH3 domain ($SH3_{[\beta1-\beta4]}$) are separated from the fifth β strand ($SH3_{[\beta5]}$) by the HOOK domain (Chen et al., 2004; Opatowsky et al., 2004; Van Petegem et al., 2004), and the relevant amino acids required for binding to PxxPs motif are concealed (Chen et al., 2004, 2009). However, the corresponding β3-$SH3_{(\beta1-\beta4)}$-HOOK-$SH3_{(\beta5)}$ was sufficient to interact with the IP_3R (Figure 4) and functioned as the specific protein-interaction module. The β3 interacts with a number of other proteins in addition to the ion-conducting α1 pores of high-Cavs and the IP_3R. Part of its GK domain enables interaction with monomeric GTP-binding proteins (Béguin et al., 2001, 2007; Buraei and Yang, 2013; Yang and Colecraft, 2013). It interacts with and suppresses the transcriptional activity of an isoform of Pax6 in *Xenopus* oocytes (Zhang et al., 2010). It also binds to the BARP in PC12 cells (Béguin et al., 2014), which modulates the localization of β and its association with the Cavα1 pore to negatively regulate the Cav activity. The region in β3 responsible for binding to BARP and PAX6 has not been identified but may involve the $SH3_{(\beta1-\beta4)}$-HOOK-$SH3_{(\beta5)}$ domain.

The binding sites of IP_3Rs for several specific protein ligands have been described (Prole and Taylor, 2016). The proteins bound by the IP3R's N terminus, which comprises the cytoplasmic suppressor domain and IP_3-binding core, include homer, calmodulin, Ca^{2+} binding protein 1 (CaBP1), RACK1, and the IP_3R-binding protein released with IP_3 (IRBIT). IRBIT competes with IP_3 for binding to the same site on IP_3Rs (Ando et al., 2003, 2006), whereas RACK1 has been shown to physiologically bind IP_3Rs and regulates Ca^{2+} release by enhancing IP_3R binding affinity for IP_3 (Patterson et al., 2004). The β3 subunit decreased the affinity of IP_3 to the IP_3R independently of receptor activation. IP_3Rs share structural and sequence homology with other Ca^{2+} release channels of the ER, the ryanodine receptors (RyR) (Efremov et al., 2015), which also interact with a Ca^{2+} channel β subunit. Physical interaction of the RyR type 1 (RyR1) with the dihydropyridine receptor Cav1.1 (α1 s) triggers excitation-contraction coupling in skeletal muscle, and the β1a subunit of the Cav1.1 calcium channel may have a direct role in the transmission of the signal from the voltage sensor (α1 s) to the calcium release channel (RyR1) (Flucher et al., 2005; Szpyt et al., 2012) by directly interacting with the RyR1 (Cheng et al., 2005; Rebbeck et al., 2015).

In the presence of β3, the *in vitro* motility of fibroblasts is significantly reduced compared with cells lacking β3, whereas phosphorylation of MLCs and FAK as well as collagen secretion is increased in the latter cells, most probably because of increased cytoplasmic [Ca^{2+}] (Figures 6A–6F). The β3 protein is present in skin fibroblasts from wild-type mice (Figure 6G). These fibroblasts are proliferating and are attracted to migrate toward the wound area either from the edge of the wound or from the bone marrow during repair of skin wounds (Gurtner et al., 2008). Using the skinfold chamber model (Sorg et al., 2007), we therefore studied wound healing in wild-type and β3 KO mice. The advantages of the skinfold chamber are manifold. First, it prevents skin contraction, which impedes following wound healing in mice. Second, it allows covering the wound with a glass coverslip, curtailing desiccation and tissue trauma, which might delay the healing process. Third, wound healing can be continuously followed under the microscope, as shown in Figure 6H. Our data show that the skin wound healing is accelerated in β3 KO mice, especially during the remodeling phase (days 6–14), when fibroblast migration into the wound and collagen secretion predominate. At day 10, the wounds in β3 KO mice were almost completely closed compared with the wounds in wild-type controls, which showed wound healing and epithelialization over 14 days similar as previously described (Eming et al., 2007). At 6 days post-wounding, only a minor but significant acceleration of wound repair in β3 KO mice was detectable. The β3 KO $CD8^+$ T lymphocytes show a survival defect (Jha et al., 2009) and might contribute to the wound repair during this initial inflammatory phase.

The spatiotemporal signature of cytoplasmic [Ca^{2+}] is crucial for physiological responses: in the rather sedentary primary fibroblasts, as shown here, the increase of cytoplasmic [Ca^{2+}] relies mainly on Ca^{2+} release from the ER. This release is tightly controlled, and the β3, unrelated to its function as a Ca^{2+} channel subunit, adds to this control. This finding is in contrast to other cells such as lymphocytes, in which cytoplasmic Ca^{2+} signals significantly rely on store-operated Ca^{2+} currents, which are absent in fibroblasts, as shown in Figures S2E and S2F.

In conclusion, our study demonstrates that the β3 subunit specifically fine-tunes the agonist-induced IP_3R response independently of its function as a Cav subunit. Modification of the IP_3R's sensitivity to IP_3 might well be the underlying mechanism for the observed phenotype of accelerated skin wound healing and for the previous observations of enhanced glucose clearance (Berggren et al., 2004) in β3 KO mice. Accordingly, targeted therapies to impair β3/IP_3R interaction might be beneficial in diabetes and delayed skin wound healing.

EXPERIMENTAL PROCEDURES

Animals and Ethics Statement

Cacnb3$^{-/-}$ mice (Murakami et al., 2002) were generated by targeting part of exon 3, exon 4, and part of the adjacent intron of the *Cacnb3* gene, thereby preventing translation of β strands 2–5 of the SH3 domain and of all β3 protein sequences C-terminal of the SH3 domain from the recombinant allele. Mice were backcrossed more than ten generations to C57BL/6 mice (obtained from Charles River). Age-matched 8- to 12-week-old males were studied in wound-healing experiments. All experimental procedures were approved and performed in accordance with the ethic regulations and the animal welfare committees of Saarland University and Saarland state (AZ C1-2.4.2.2/16-2015). All efforts were made to minimize animal suffering and to reduce the number of animals used.

Isolation of Primary Cells, Cell Culture, and Transfection

Fibroblasts were prepared from mouse embryos at embryonic day 14.5 from pregnant female C57BL/6 wild-type and *Cacnb3*$^{-/-}$ mice, as previously described (Fischer et al., 2013), and used up to passage 5. Cos-7 and HEK

cells (ATCC CRL-1651 and CRL-1573) were grown in DMEM and minimum essential medium (MEM), respectively, supplemented with 1% GlutaMAX (Cos-7) and 10% fetal calf serum (all from GIBCO by Life Technologies, Paisley, UK), and maintained at 37°C and 5% CO_2. Cell transfection was performed using Fugene HD (Promega, Madison, Wisconsin, USA). All cDNAs used in this study are listed in Table S1. Further details are provided Supplemental Experimental Procedures.

Immunoprecipitation and Western Blot

Cells were lysed in a buffer containing 50 mM HEPES, 150 mM NaCl, 1 mM $CaCl_2$, 1% (w/v) digitonin, and protease inhibitors for 1 hr at 4°C under rotation. After centrifugation at 100,000 × *g* for 45 min at 4°C, the supernatant was incubated with the corresponding antibody coupled to magnetic beads (Dynabeads; Invitrogen by Life Technologies, Oslo, Norway) for 2 hr at 4°C under end-over-end rotation. Subsequently, beads were extensively washed, and proteins bound by the beads were eluted thereafter in the presence of SDS-denaturing buffer, run on SDS-PAGE, transferred to nitrocellulose, probed with the indicated antibodies, and visualized by secondary antibodies conjugated to horseradish peroxidase after the addition of the Western lightning chemiluminescence reagent plus (PerkinElmer, Waltham, MA, USA) at the LAS-3000 analyzer (Fujifilm). Antibodies used in this study are listed in Table S2.

Measurements of Cytoplasmic Ca^{2+} by Fura-2

Cells were cultured on poly-L-lysine (Sigma-Aldrich, Steinheim, Germany) coated glass coverslips and loaded with 5 μM Fura-2 AM (Invitrogen by Thermo Fisher Scientific, Eugene, Oregon, USA) for 45 min at 37°C in the dark. Every 2 s, Fura-2 was alternately excited (0.5 Hz) at 340 and 380 nm for 20 ms, and the emitted fluorescence was recorded. After background correction, ratio images were calculated from 340 and 380 nm images. Calibration indicate that the Ca^{2+} concentration remains close to the effective K_d of Fura-2, as outlined in detail in Supplemental Experimental Procedures.

IP_3 Flash Photolysis

Cells (Cos-7 cells transfected with the Cavβ3 cDNA and non-transfected or fibroblasts from wild-type and β3 KO mice) were plated on the same glass coverslip (Figure S3), to warrant equal Fluo-4/AM (1 μM) and caged IP_3 (3 μM membrane-permeable caged "ci-IP_3/PM") loading for 40 min. Then, glass coverslips were placed into a circular open-bottom chamber and supplemented with 200 μL Tyrode's solution. Fluo-4 was excited with the 491 nm laser, and emission was collected through a 515 nm long-pass filter. Images were recorded at 2 frames/s, and uncaging of IP_3 was obtained by UV flashes.

Preparation of Mouse Cerebellar Membranes and IP_3 Binding Assays

Mouse cerebellar membranes were prepared according to (Yoshikawa et al., 1999) and used for equilibrium binding of [^{3}H]IP_3 (19.30 Ci/mmol; PerkinElmer, Boston, MA, USA) for 30 min at 4°C in a total volume of 0.1 mL of buffer A (50 mM Tris-HCl, 1 mM EDTA, 1 mM DTT [pH 8.30]) containing protease inhibitors. The reaction was stopped by centrifugation at 16,000 × *g* at 4°C for 10 min, and the supernatant containing unbound [^{3}H]IP_3 was discarded. The pellet was washed twice with ice-cold buffer A, resuspended in 0.2 mL H_2O, added to 4.5 mL scintillation cocktail (Zinsser Analytic UNISAFE1, Berkshire, UK), and subjected to liquid scintillation counting (WALLAC 1409 counter). Using purified recombinant proteins, 1.5 μM IP_3-receptor type 3 binding domain fused to GST (IP_3BD aa 224–604), and Cavβ3-GST or GST alone (at 30–300 nM each) were preincubated in buffer A for 10 min at 4°C; then, [^{3}H]IP_3 (10 nM) was added, yielding a total volume of 0.1 mL. After 10 min incubation at 4°C, the reaction was stopped by addition of 3 mL ice-cold solution B (50 mM Tris-HCl, 1 mM EDTA, 1 mM DTT, 12% w/v polyethylene glycol 8000, 1.2 mg/mL BSA [pH 8.3]) containing protease inhibitors. The suspension was immediately poured on GF/C filters. After washing three times with solution B, the filter was subjected to liquid scintillation counting as detailed above.

Scratch Migration Assay and Skin Wound Healing Using the Mouse Dorsal Skinfold Chamber

Fibroblasts were plated on glass slides at a cell density of 6 × 10^5 cells per slide in complete media and cultured for 24 hr. Next day, at time point 0, a 200 μL pipette tip was used to perform scratches over the confluent monolayer. Cell migration was observed for 30 hr by phase contrast microscopy (BZ-8000; Keyence, Osaka, Japan).

Implantation of the dorsal skinfold chamber and wounding were performed as previously described (Sorg et al., 2007). The dermal wound (2 mm in diameter) was applied with a biopsy punch (pfm Medical, Köln, Germany) at one side of the skinfold by removing the complete skin with epidermis and dermis. The final wound area covered 3.5–4.5 mm^2. To monitor skin wound repair, mice were anesthetized and placed on a custom made Plexiglas platform, which was put under a stereomicroscope. Images were taken with different magnifications. At the time points indicated, the size of the wound area was determined and plotted as percentage of the wound area immediately after injury.

Collagen Secretion

Collagen in conditioned media was measured using a Sircol Collagen Assay (Biocolor, Carrickfergus, Northern Irland, UK) following the manufacturer's protocol.

Statistical Analyses

Data analyses were performed using GraphPad Prism version 6.07 (GraphPad Software, La Jolla, CA), Microsoft Excel, Igor Pro 5.1 (WaveMetrics), TILLvisION (TILL Photonics), and AIDA Image Analyzer version 4.14. Data are presented as mean ± SEM and were tested for normality using D'Agostino-Pearson omnibus or Shapiro-Wilk normality tests. For single comparisons between two groups, unpaired two-tailed Student's t test or Mann-Whitney test was used as indicated. For comparisons between three or more groups, one- or two-way ANOVA followed by Bonferroni's multiple-comparisons test was used, as indicated in the corresponding figure legend. p values < 0.05 were considered to indicate statistical significance.

SUPPLEMENTAL INFORMATION

Supplemental Information includes Supplemental Experimental Procedures, six figures, and two tables and can be found with this article online at https://doi.org/10.1016/j.celrep.2018.01.010.

ACKNOWLEDGMENTS

We thank Dr. Petra Weissgerber and the Transgene Unit of the SPF animal facility (project P2 of SFB 894) of the Medical Faculty, Homburg. We thank Stefanie Buchholz, Christine Wesely, Karin Wolske, and Martin Simon-Thomas for excellent technical assistance and Dr. Adolfo Cavalié (all Pharmacology Homburg, Germany) for helpful discussion. This study was funded by Deutsche Forschungsgemeinschaft (DFG) SFB 894 (A. Beck, P.L., and V.F.) and DFG/IRTG1830 (A. Belkacemi).

AUTHOR CONTRIBUTIONS

A. Belkacemi performed all experiments and together with A. Beck and V.F. conceived all experiments. A. Beck and B.W. performed patch-clamp experiments. X.H. and P.L. conceived and performed experiments with uncaging IP_3. U.W. cloned and provided the cDNAs of murine IP_3R types 1, 2, and 3. M.W.L. and M.D.M. introduced the skinfold chamber and supported A. Belkacemi when performing the *in vivo* wound experiments. A. Belkacemi, A. Beck, M.W.L., and P.L. edited the manuscript. V.F. contributed to all aspects of the manuscript (provided expertise, supervision, review, and wrote and edited the manuscript).

DECLARATION OF INTERESTS

The authors declare no competing interests. V.F. participates in a patent on β3 subunit as potential drug target in diabetes.

Received: November 3, 2017
Revised: December 10, 2017
Accepted: January 3, 2018
Published: January 30, 2018

REFERENCES

Ando, H., Mizutani, A., Matsu-ura, T., and Mikoshiba, K. (2003). IRBIT, a novel inositol 1,4,5-trisphosphate (IP3) receptor-binding protein, is released from the IP3 receptor upon IP3 binding to the receptor. J. Biol. Chem. *278*, 10602–10612.

Ando, H., Mizutani, A., Kiefer, H., Tsuzurugi, D., Michikawa, T., and Mikoshiba, K. (2006). IRBIT suppresses IP3 receptor activity by competing with IP3 for the common binding site on the IP3 receptor. Mol. Cell *22*, 795–806.

Béguin, P., Nagashima, K., Gonoi, T., Shibasaki, T., Takahashi, K., Kashima, Y., Ozaki, N., Geering, K., Iwanaga, T., and Seino, S. (2001). Regulation of Ca^{2+} channel expression at the cell surface by the small G-protein kir/Gem. Nature *411*, 701–706.

Béguin, P., Ng, Y.J., Krause, C., Mahalakshmi, R.N., Ng, M.Y., and Hunziker, W. (2007). RGK small GTP-binding proteins interact with the nucleotide kinase domain of Ca2+-channel beta-subunits via an uncommon effector binding domain. J. Biol. Chem. *282*, 11509–11520.

Béguin, P., Nagashima, K., Mahalakshmi, R.N., Vigot, R., Matsunaga, A., Miki, T., Ng, M.Y., Ng, Y.J., Lim, C.H., Tay, H.S., et al. (2014). BARP suppresses voltage-gated calcium channel activity and Ca2+-evoked exocytosis. J. Cell Biol. *205*, 233–249.

Berggren, P.O., Yang, S.N., Murakami, M., Efanov, A.M., Uhles, S., Köhler, M., Moede, T., Fernström, A., Appelskog, I.B., Aspinwall, C.A., et al. (2004). Removal of Ca^{2+} channel beta3 subunit enhances Ca^{2+} oscillation frequency and insulin exocytosis. Cell *119*, 273–284.

Buraei, Z., and Yang, J. (2010). The ß subunit of voltage-gated Ca2+ channels. Physiol. Rev. *90*, 1461–1506.

Buraei, Z., and Yang, J. (2013). Structure and function of the β subunit of voltage-gated Ca^{2+} channels. Biochim. Biophys. Acta *1828*, 1530–1540.

Catterall, W.A., Perez-Reyes, E., Snutch, T.P., and Striessnig, J. (2005). International Union of Pharmacology. XLVIII. Nomenclature and structure-function relationships of voltage-gated calcium channels. Pharmacol. Rev. *57*, 411–425.

Chen, Y.H., Li, M.H., Zhang, Y., He, L.L., Yamada, Y., Fitzmaurice, A., Shen, Y., Zhang, H., Tong, L., and Yang, J. (2004). Structural basis of the alpha1-beta subunit interaction of voltage-gated Ca^{2+} channels. Nature *429*, 675–680.

Chen, Y.H., He, L.L., Buchanan, D.R., Zhang, Y., Fitzmaurice, A., and Yang, J. (2009). Functional dissection of the intramolecular Src homology 3-guanylate kinase domain coupling in voltage-gated Ca2+ channel beta-subunits. FEBS Lett. *583*, 1969–1975.

Cheng, W., Altafaj, X., Ronjat, M., and Coronado, R. (2005). Interaction between the dihydropyridine receptor Ca2+ channel beta-subunit and ryanodine receptor type 1 strengthens excitation-contraction coupling. Proc. Natl. Acad. Sci. U S A *102*, 19225–19230.

Dolphin, A.C. (2012). Calcium channel auxiliary α2δ and β subunits: trafficking and one step beyond. Nat. Rev. Neurosci. *13*, 542–555.

Efremov, R.G., Leitner, A., Aebersold, R., and Raunser, S. (2015). Architecture and conformational switch mechanism of the ryanodine receptor. Nature *517*, 39–43.

Eming, S.A., Werner, S., Bugnon, P., Wickenhauser, C., Siewe, L., Utermöhlen, O., Davidson, J.M., Krieg, T., and Roers, A. (2007). Accelerated wound closure in mice deficient for interleukin-10. Am. J. Pathol. *170*, 188–202.

Etemad, S., Obermair, G.J., Bindreither, D., Benedetti, A., Stanika, R., Di Biase, V., Burtscher, V., Koschak, A., Kofler, R., Geley, S., et al. (2014). Differential neuronal targeting of a new and two known calcium channel β4 subunit splice variants correlates with their regulation of gene expression. J. Neurosci. *34*, 1446–1461.

Fan, M., Zhang, W.K., Buraei, Z., and Yang, J. (2012). Molecular determinants of Gem protein inhibition of P/Q-type Ca2+ channels. J. Biol. Chem. *287*, 22749–22758.

Fan, G., Baker, M.L., Wang, Z., Baker, M.R., Sinyagovskiy, P.A., Chiu, W., Ludtke, S.J., and Serysheva, I.I. (2015). Gating machinery of InsP3R channels revealed by electron cryomicroscopy. Nature *527*, 336–341.

Fell, B., Eckrich, S., Blum, K., Eckrich, T., Hecker, D., Obermair, G.J., Münkner, S., Flockerzi, V., Schick, B., and Engel, J. (2016). α2δ2 controls the function and trans-synaptic coupling of Cav1.3 channels in mouse inner hair cells and is essential for normal hearing. J. Neurosci. *36*, 11024–11036.

Fischer, M., Horn, S., Belkacemi, A., Kojer, K., Petrungaro, C., Habich, M., Ali, M., Küttner, V., Bien, M., Kauff, F., et al. (2013). Protein import and oxidative folding in the mitochondrial intermembrane space of intact mammalian cells. Mol. Biol. Cell *24*, 2160–2170.

Flucher, B.E., Obermair, G.J., Tuluc, P., Schredelseker, J., Kern, G., and Grabner, M. (2005). The role of auxiliary dihydropyridine receptor subunits in muscle. J. Muscle Res. Cell Motil. *26*, 1–6.

Freise, D., Himmerkus, N., Schroth, G., Trost, C., Weissgerber, P., Freichel, M., and Flockerzi, V. (1999). Mutations of calcium channel beta subunit genes in mice. Biol. Chem. *380*, 897–902.

Gurtner, G.C., Werner, S., Barrandon, Y., and Longaker, M.T. (2008). Wound repair and regeneration. Nature *453*, 314–321.

Hamada, K., Miyatake, H., Terauchi, A., and Mikoshiba, K. (2017). IP3-mediated gating mechanism of the IP3 receptor revealed by mutagenesis and X-ray crystallography. Proc. Natl. Acad. Sci. U S A *114*, 4661–4666.

He, L.L., Zhang, Y., Chen, Y.H., Yamada, Y., and Yang, J. (2007). Functional modularity of the beta-subunit of voltage-gated Ca2+ channels. Biophys. J. *93*, 834–845.

Held, B., Tsvilovskyy, V., Meissner, M., Kaestner, L., Ludwig, A., Mossmang, S., Lipp, P., Freichel, M., and Flockerzi, V. (2007). Ca^{2+} channel currents and contraction in CaVbeta3-deficient ileum smooth muscle from mouse. Cell Calcium *42*, 477–487.

Hibino, H., Pironkova, R., Onwumere, O., Rousset, M., Charnet, P., Hudspeth, A.J., and Lesage, F. (2003). Direct interaction with a nuclear protein and regulation of gene silencing by a variant of the Ca2+-channel beta 4 subunit. Proc. Natl. Acad. Sci. U S A *100*, 307–312.

Hofmann, F., Flockerzi, V., Kahl, S., and Wegener, J.W. (2014). L-type CaV1.2 calcium channels: from in vitro findings to in vivo function. Physiol. Rev. *94*, 303–326.

Jeon, D., Song, I., Guido, W., Kim, K., Kim, E., Oh, U., and Shin, H.S. (2008). Ablation of Ca^{2+} channel beta3 subunit leads to enhanced N-methyl-D-aspartate receptor-dependent long term potentiation and improved long term memory. J. Biol. Chem. *283*, 12093–12101.

Jha, M.K., Badou, A., Meissner, M., McRory, J.E., Freichel, M., Flockerzi, V., and Flavell, R.A. (2009). Defective survival of naive CD8+ T lymphocytes in the absence of the beta3 regulatory subunit of voltage-gated calcium channels. Nat. Immunol. *10*, 1275–1282.

Kadurin, I., Ferron, L., Rothwell, S.W., Meyer, J.O., Douglas, L.R., Bauer, C.S., Lana, B., Margas, W., Alexopoulos, O., Nieto-Rostro, M., et al. (2016). Proteolytic maturation of α2δ represents a checkpoint for activation and neuronal trafficking of latent calcium channels. eLife *5*, 5.

Kim, D.I., Kang, M., Kim, S., Lee, J., Park, Y., Chang, I., and Suh, B.C. (2015). Molecular basis of the membrane interaction of the β2e subunit of voltage-gated Ca(2+) channels. Biophys. J. *109*, 922–935.

Link, S., Meissner, M., Held, B., Beck, A., Weissgerber, P., Freichel, M., and Flockerzi, V. (2009). Diversity and developmental expression of L-type calcium channel beta2 proteins and their influence on calcium current in murine heart. J. Biol. Chem. *284*, 30129–30137.

Ludwig, A., Flockerzi, V., and Hofmann, F. (1997). Regional expression and cellular localization of the alpha1 and beta subunit of high voltage-activated calcium channels in rat brain. J. Neurosci. *17*, 1339–1349.

Miranda-Laferte, E., Ewers, D., Guzman, R.E., Jordan, N., Schmidt, S., and Hidalgo, P. (2014). The N-terminal domain tethers the voltage-gated calcium channel β2e-subunit to the plasma membrane via electrostatic and hydrophobic interactions. J. Biol. Chem. *289*, 10387–10398.

Müller, C.S., Haupt, A., Bildl, W., Schindler, J., Knaus, H.G., Meissner, M., Rammner, B., Striessnig, J., Flockerzi, V., Fakler, B., and Schulte, U. (2010). Quantitative proteomics of the Cav2 channel nano-environments in the mammalian brain. Proc. Natl. Acad. Sci. U S A *107*, 14950–14957.

Murakami, M., Fleischmann, B., De Felipe, C., Freichel, M., Trost, C., Ludwig, A., Wissenbach, U., Schwegler, H., Hofmann, F., Hescheler, J., et al. (2002). Pain perception in mice lacking the beta3 subunit of voltage-activated calcium channels. J. Biol. Chem. *277*, 40342–40351.

Namkung, Y., Smith, S.M., Lee, S.B., Skrypnyk, N.V., Kim, H.L., Chin, H., Scheller, R.H., Tsien, R.W., and Shin, H.S. (1998). Targeted disruption of the Ca2+ channel beta3 subunit reduces N- and L-type Ca2+ channel activity and alters the voltage-dependent activation of P/Q-type Ca2+ channels in neurons. Proc. Natl. Acad. Sci. U S A *95*, 12010–12015.

Opatowsky, Y., Chen, C.C., Campbell, K.P., and Hirsch, J.A. (2004). Structural analysis of the voltage-dependent calcium channel beta subunit functional core and its complex with the alpha 1 interaction domain. Neuron *42*, 387–399.

Park, C.G., Park, Y., and Suh, B.C. (2017). The HOOK region of voltage-gated Ca2+ channel β subunits senses and transmits PIP2 signals to the gate. J. Gen. Physiol. *149*, 261–276.

Patterson, R.L., van Rossum, D.B., Barrow, R.K., and Snyder, S.H. (2004). RACK1 binds to inositol 1,4,5-trisphosphate receptors and mediates Ca2+ release. Proc. Natl. Acad. Sci. U S A *101*, 2328–2332.

Prole, D.L., and Taylor, C.W. (2016). Inositol 1,4,5-trisphosphate receptors and their protein partners as signalling hubs. J. Physiol. *594*, 2849–2866.

Putney, J.W., Jr., and Bird, G.S. (1993). The inositol phosphate-calcium signaling system in nonexcitable cells. Endocr. Rev. *14*, 610–631.

Qin, N., Platano, D., Olcese, R., Costantin, J.L., Stefani, E., and Birnbaumer, L. (1998). Unique regulatory properties of the type 2a Ca^{2+} channel beta subunit caused by palmitoylation. Proc. Natl. Acad. Sci. U S A *95*, 4690–4695.

Rebbeck, R.T., Willemse, H., Groom, L., Casarotto, M.G., Board, P.G., Beard, N.A., Dirksen, R.T., and Dulhunty, A.F. (2015). Regions of ryanodine receptors that influence activation by the dihydropyridine receptor β1a subunit. Skelet. Muscle *5*, 23.

Rima, M., Daghsni, M., Fajloun, Z., M'rad, R., Brusés, J.L., Ronjat, M., and De Waard, M. (2016). Protein partners of the calcium channel β subunit highlight new cellular functions. Biochem. J. *473*, 1831–1844.

Sixt, M. (2012). Cell migration: fibroblasts find a new way to get ahead. J. Cell Biol. *197*, 347–349.

Sorg, H., Krueger, C., and Vollmar, B. (2007). Intravital insights in skin wound healing using the mouse dorsal skin fold chamber. J. Anat. *211*, 810–818.

Suh, B.C., Kim, D.I., Falkenburger, B.H., and Hille, B. (2012). Membrane-localized β-subunits alter the PIP2 regulation of high-voltage activated Ca2+ channels. Proc. Natl. Acad. Sci. U S A *109*, 3161–3166.

Szpyt, J., Lorenzon, N., Perez, C.F., Norris, E., Allen, P.D., Beam, K.G., and Samsó, M. (2012). Three-dimensional localization of the α and β subunits and of the II-III loop in the skeletal muscle L-type Ca2+ channel. J. Biol. Chem. *287*, 43853–43861.

Tadmouri, A., Kiyonaka, S., Barbado, M., Rousset, M., Fablet, K., Sawamura, S., Bahembera, E., Pernet-Gallay, K., Arnoult, C., Miki, T., et al. (2012). Cacnb4 directly couples electrical activity to gene expression, a process defective in juvenile epilepsy. EMBO J. *31*, 3730–3744.

Totsukawa, G., Wu, Y., Sasaki, Y., Hartshorne, D.J., Yamakita, Y., Yamashiro, S., and Matsumura, F. (2004). Distinct roles of MLCK and ROCK in the regulation of membrane protrusions and focal adhesion dynamics during cell migration of fibroblasts. J. Cell Biol. *164*, 427–439.

Van Petegem, F., Clark, K.A., Chatelain, F.C., and Minor, D.L., Jr. (2004). Structure of a complex between a voltage-gated calcium channel beta-subunit and an alpha-subunit domain. Nature *429*, 671–675.

Vogt, S., Grosse, R., Schultz, G., and Offermanns, S. (2003). Receptor-dependent RhoA activation in G12/G13-deficient cells: genetic evidence for an involvement of Gq/G11. J. Biol. Chem. *278*, 28743–28749.

Yang, T., and Colecraft, H.M. (2013). Regulation of voltage-dependent calcium channels by RGK proteins. Biochim. Biophys. Acta *1828*, 1644–1654.

Yoshikawa, F., Iwasaki, H., Michikawa, T., Furuichi, T., and Mikoshiba, K. (1999). Cooperative formation of the ligand-binding site of the inositol 1,4, 5-trisphosphate receptor by two separable domains. J. Biol. Chem. *274*, 328–334.

Zhang, Y., Yamada, Y., Fan, M., Bangaru, S.D., Lin, B., and Yang, J. (2010). The beta subunit of voltage-gated Ca2+ channels interacts with and regulates the activity of a novel isoform of Pax6. J. Biol. Chem. *285*, 2527–2536.

Zhao, X.K., Cheng, Y., Liang Cheng, M., Yu, L., Mu, M., Li, H., Liu, Y., Zhang, B., Yao, Y., Guo, H., et al. (2016). Focal adhesion kinase regulates fibroblast migration via integrin beta-1 and plays a central role in fibrosis. Sci. Rep. *6*, 19276.